Systematic Investigation of Cuttings Transport Behavior in Horizontal Drilling Operation

Nnorom Obinichi[1], Ugwulashi, Charles[2], Obioma Eseonu[3]
[1]Department of Mechanical Engineering, Faculty of Engineering, University of Port Harcourt, Choba, P.M.B., 5323, Nigeria
[2]Department of Mechanical Engineering, Faculty of Engineering, University of Port Harcourt, Choba, P.M.B., 5323, Nigeria
[3]Department of Mechanical Engineering, Faculty of Engineering, University of Port Harcourt, Choba, P.M.B., 5323, Nigeria
Corresponding Author: obinichi.nnorom@uniport.edu.ng

***Abstract*: The aim of this study is the systematic investigation of cutting transport behaviour in horizontal drilling operation and the complete workflow of this study is comprised of four tasks: appropriate design of experiment (DOE), simulation set up, experimental validation and sensitive analysis. In the DOE, all parameters used in this study are grouped according to their respective categories, where their ranges are given. The simulation setup includes drawing the geometry, meshing, and running the simulation based on proper boundary conditions. In conclusion, the increase in the elemental size in a concentric annulus, a moderately eccentric annulus and a highly eccentric annulus decreases the cuttings pressure drop for fully concentric annulus, where (e) is 0, moderately eccentric annulus, where (e) is equal to 0.4 and highly eccentric annulus, where (e) is equal to 0.7. The increase in the fluid velocity increases the annular cuttings pressure drops for non-Newtonian fluid, with no solid and no drill pipe rotation, as well as non-Newtonian fluid, with a 4% solid and a 400RPM drilling pipe rotation. The increase in average fluid velocity increases the average cuttings velocity for horizontal annulus and the increase in annular fluid velocity increases the total pressure drops of cuttings.**

***Keywords*: Drilling, fluid, cutting, annulus, transport, pressure, simulation.**

1. Introduction

The advancements in technology and the ongoing rise in the demand for fossil fuels, the petroleum industry is using horizontal, directional and extend reach drill to explore offshore, subsea and geologically harsh locations where conventional drilling operations are less practical. Drilling horizontally is now common in recent years, as a result of increased interaction for the pay reservoirs, a rise in the production rate, a decrease in the drop of pressure, and a rise in the final oil and gas output.

A spinning drill bit is used to bore the hole in a standard rotary drilling technique. A drill string is linked to the drilling bit and pushed until it reaches the top ground level. From the top, a downward heavy mass is impacted to the bit, and the drilling bit is also rotated (Huque, 2022). The contact of the drilling bits with earth formations, such as sedimentary rock, produces numerous chip particles of various shapes and sizes. A standard fluid is circulated in a drilling operation, which has a drilling fluid flow mechanism. It is injected into the wellbore via the drilling bit, and the cuttings are transported out of the hole through the annular wellbore. Gritstone cuttings are subsequently sorted out at the surface level through the use of shake shakers (vibration screens), demanders, and the mud system is then re-circulated via the wellbore as shown in Figure 1, which depicts a basic configuration system with mud fluid flow dynamics. To ensure a well-organized drilling operation, it is critical to effectively and systematically remove sandstone and chip particles from the bottom hole (Huque, 2022).

A good hole cleaning procedure is vital and important to the success of oil and gas exploration. The capacity of a drilling fluid circulating system, to remove sandstone cuttings out of the wellbore during a drilling operation is known as "hole cleaning". Poor hole cleaning can easily result in a number of expensive issues with terrible outcomes, such as clogged pipes, an increased torque, an increased drag system, fast wearing of bits, and even a sluggish penetration rate that reduces drilling time. In order to prevent these issues, more caution should be taken before drilling.

Also, rock chips are created when holes are drilled with a spinning drill bit in rotary drilling. Drilling mud is injected into the wellbore by drilling fluid circulation systems, which then convey the cuttings out. Shale shakers, desanders, etc are used to separate drill cuttings at the surface before they are recirculated back into the well bore. For drilling operations to be efficient, drill cuttings must be removed effectively.

Laboratory studies and field encounters have demonstrated that inclined or horizontal wells, where drilling cutting have a tendency to settle in the lower session, have serious whole cleaning issues. The removal of cuttings from a horizontal or inclined wells has problems that are not present in a vertical well or wells that are nearly vertical (Huque, 2022). The issues of cuttings removal are always evident in wells that deviates from the vertical by around 30 degrees. Therefore, for directional, extended reach, near horizontal and horizontal wells, appropriate well cleaning should be used throughout the drilling process. To increase the removal of rock particle that were cut during drilling, a suitable circulation fluid design and the knowledge of the drilling fluid's transport capabilities may be the answer.

A. *Solid-Liquid Flow*

Drilling mud and solid cuttings move in two phases during transportation of cuttings in the annulus. The two-phase flow system in this work is modeled using the Eulerian-Eulerian multi-phase flow model (Inc. ANSYS, 2013). Cuttings are regarded as the secondary fluid and drilling mud as the primary fluid. Solid cuts in the Eulerian-Eulerian model are handled as a continuum. Figure 2.1 shows a basic concentric and eccentric drill pipe schematiz designs and illustrates an ideal system for drilling cuttings transportation.

The two-phase model takes into account the following presumptions.

- Non-Newtonian incompressible drilling fluid. The fluid properties and behaviors are represented by a Herschel-Bulkley model.
- Every drill cutting has a mean diameter and is a sphere.
- Drill cuttings have a consistent density.
- The interface has no mass transfer between the cuttings and drilling mud.
- The pressure is the same in both phases; the distribution of pressure is consistent across all phases.
- A preserved isothermal state.

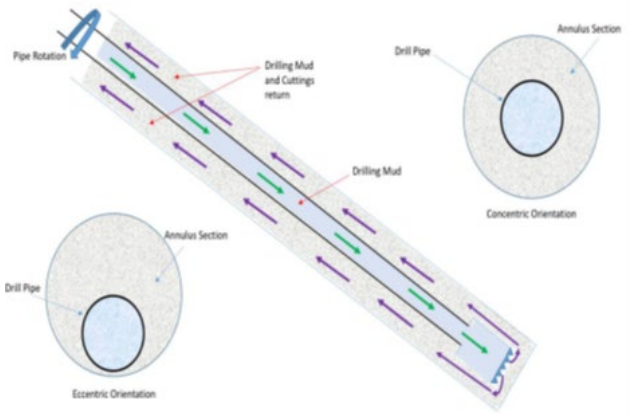

Fig. 1. Illustrates the transportation of cuttings in an annular section with both the concentric and eccentric profiles

According to Wei et al. (2018), the eccentricity of the pipe is defined as follows:

$$e = 2\delta/(D\_hole-D\_pipe) \quad (1)$$

Where **ρ** denotes the annulus' eccentricity and δ the offset from the center. The hole and pipe diameters are denoted by $Dole$ and $Dpipe$, respectively.

B. *Mass conservation*

The following is the equation of continuity for the liquid drilling mud (Fluent, 2015):

The equation of continuity for the drilling mud (liquid) is given below (Fluent, 2015):

$$\frac{\partial}{\partial t}(\alpha_l\rho_l) + \nabla.(\alpha_l\rho_l\overrightarrow{v_l} = \sum(\dot{m}_{ls} - \dot{m}_{sl}) \quad (2)$$

This shows that Bl represents the liquid phase's density and vl represents its velocity; Mass transfer going from the liquid phase to the solid phase is referred to as mls, while mass transfer from the solid phase to the liquid phase is similar to mre. The addition on the right-hand side of Equation (2) is taken to be zero since there is no mass transfer between the phases. There are only two phases in the circular volume. For the mud phase, the volume percentage is αl, and for the cuttings, it is αs, where αl+αs =1. The phases of mud (liquid) and cuts (solid) are denoted by the subscripts 1 and s, respectively. Similarly, the following represents the continuity equation for the solid phasing: connection (Fluent, 2015)):

$$\frac{\partial}{\partial t}(\alpha_s\rho_s) + \nabla.(\alpha_s\rho_s\overrightarrow{v_s} = \sum(\dot{m}_{ls} - \dot{m}_{sl}) = 0 \quad (3)$$

Where, v_s is the solid phase velocity;

ρ_s stands for the solid phase density.

C. *Conservation of momentum*

The following equations states the momentum balance for the liquid phase (Fluent, 2015):

$$\frac{\partial}{\partial t}(\alpha_l\rho_l\overrightarrow{v_l}) + \nabla.(\alpha_l\rho_l\overrightarrow{v_l}\,\overrightarrow{v_l}) = -\alpha_l\nabla_p + \nabla.\overline{\overline{\tau_l}} + \alpha_l\rho_l\vec{g} + \sum\overrightarrow{R_{sl}} + \dot{m}_{sl}\overrightarrow{v_{sl}} - \dot{m}_{ls}\overrightarrow{v_{ls}} + (\overrightarrow{F_l} + \overrightarrow{F_{lift,l}} + \overrightarrow{F_{wl,l}} + \overrightarrow{F_{vm,l}} + \overrightarrow{F_{td,l}}) \quad (4)$$

Where,

$\overrightarrow{F_l}$ (External body force)

$\overrightarrow{F_{lift,l}}$ (Lift force)

$\overrightarrow{F_{wl,l}}$ (Wall lubrication force)

$\overrightarrow{F_{vm,l}}$ (Virtual mass force)

$F\,td,$ (Turbulent dispersion force)

p (Pressure shared by both solid and liquid phases)

$\overrightarrow{v_{sl}}$ (Inter-phase velocity defined as: $\overrightarrow{v_{sl}} = \overrightarrow{v_s}$ if $\dot{m}_{sl} < 0$)

$\overline{\overline{\tau_l}}$ The stress-strain tensor for the liquid phase, as defined below (Fluent, 2015):

$$\overline{\overline{\tau_l}} = \alpha_l\mu_l(\nabla\overrightarrow{V_l} + \nabla\overrightarrow{V_l}\tau) + \alpha_l(\lambda_l - \tfrac{2}{3}\mu_l)\nabla\overrightarrow{V_l}\overline{\overline{I}} \quad (5)$$

From Equation (5), μ_l and λ_l denote the viscosity of shear and bulk in liquid phase, respectively.

The momentum conservation for the solid phase is expressed as follows (Fluent, 2015):

$$\frac{\partial}{\partial t}(\alpha_s\rho_s\overrightarrow{v_s}) + \nabla.(\alpha_s\rho_s\overrightarrow{v_s}\overrightarrow{v_l}) = -\alpha_l\nabla_p - \nabla.P_s + \nabla\overline{\overline{\tau_s}} + \alpha_s\rho_s\vec{g} + \sum K_{ls}(\overrightarrow{V_l} - \overrightarrow{V_s}) + \dot{m}_{ls}\overrightarrow{v_{ls}} - \dot{m}_{sl}\overrightarrow{v_{sl}} + (\overrightarrow{F_s} + \overrightarrow{F_{lift,s}} + \overrightarrow{F_{wl,s}} + \overrightarrow{F_{vm,s}} + \overrightarrow{F_{td,s}}) \quad (6)$$

where p_s is the solid phase pressure. $\overrightarrow{R_{sl}}$ is the interactive force between the solid and liquid phases. This force mainly depends on the friction and pressure cohesion and is subject to the condition that $\overrightarrow{R_{sl}} = -\overrightarrow{R_{ls}}$ and $\overrightarrow{R_u} = 0$ (Fluent, 2015), as given below:

$$\sum\overrightarrow{R_{sl}} = (\sum K_{sl}(\overrightarrow{V_s} - \overrightarrow{V_l}) = 0 \quad (7)$$

Here, K_{sl} $(= K_{sl})$ introduces the interphase momentum exchange coefficient; and $\overrightarrow{v_s}$ and $\overrightarrow{v_l}$ are the solid and liquid phase velocities, respectively.

D. *Solid Shear Stress*

In a two-phase flow, the viscosities of shear and bulk resulting from particle momentum exchange from collision between the particles are contained in the solid stress tensor. According to Fluent (2015), the combination of the collisional,

kinetic, and frictional components is the correct definition of solid shear viscosity (μs):

$$\mu_s = \mu_{s,col} + \mu_{s,kin} + \mu_{s,fr} \quad (8)$$

The formula for the collisional component of the shear viscosity (μs) was put out by Gidaspow (2014):

$$\mu_{s,col} = \frac{4}{5}\alpha_s p_s d_s g_{o,ss}(1+e_{ss})\left(\frac{\theta_s}{\pi}\right)^{\frac{1}{2}}\alpha_s \quad (9)$$

Where es stands for the coefficient of restitution and represents a distribution function; in which is the solid diameter; indicates the granular temperature of the solid phase. The following is how the solid's kinetic viscosity is introduced (Gidaspow, 2014):

$$\mu_{s,kin} = \frac{10\rho_s d_s\sqrt{\theta_s\pi}}{96\alpha_s(1+e_{ss})g_{o,ss}}\left[1+\frac{4}{5}g_{o,ss}\alpha_s(1+e_{ss})\right]^2\alpha_s \quad (10)$$

Schaeffer (2019) proposed the expression for the frictional viscosity ($\mu_{s,fr}$):

$$\mu_{s,fr} = \frac{\rho_s \sin\emptyset}{2\sqrt{I_2 D}} \quad (11)$$

Where $\emptyset$ is the internal friction angle which represents the solids pressure, and thus, presents the second deviatory stress tensor version.

$$\lambda_s = \frac{4}{5}\alpha_s{}^2\rho_s d_s g_{o,ss}(1+e_{ss})\left(\frac{\theta_s}{\pi}\right)^{\frac{1}{2}} \quad (12)$$

Model of particle drag. The interphase exchange coefficient serves as the foundation for the momentum transfer between the liquid and solid phases. The following equations (fork_{sl}), which are composites and the Ergun correlations, were first presented by (Fluent, 2015)

The fluid-solid exchange coefficient (k_{sl}) is as follows when > 0.8 (Fluent, 2015):

$$k_{sl} = \frac{3}{4}C_D\frac{\alpha_s\alpha_l\rho_l|\vec{V_s}-\vec{V_l}|}{d_s}\alpha_l{}^{-2.65} \quad (13)$$

In Equation (13), C_D is the drag coefficient that can be defined as follows:

$$C_D = \frac{24}{\alpha_l Re_s}[1+0.15(\alpha_l Re_s)^{0.687}] \; for \; Res < 1000 \quad (14)$$

and C_D=0.44 for Res >1000

$$Re_s = \frac{d_s\rho_l|\vec{V_s}-\vec{V_l}|}{\mu_l} \quad (15)$$

in which, Res is the relative Reynolds number.

When α_l < 0.8, the fluid to solid exchange coefficient and it is ascertained by the following expression:

$$k_{sl} = 150\frac{\alpha_s(1-\alpha_l)\mu_l}{\alpha_l d_s{}^2} + 1.75 + \frac{\alpha_l\alpha_s|\vec{V_s}-\vec{V_l}|}{d_s} \quad (16)$$

E. Particle Lift Model

The Saffman-Mei particle lift model is used in the ANSYS Fluent. Saffman (2019) defined the lift coefficient (C_l) for low Reynolds number flow past a spherical particle as given below:

$$C_l = \frac{3}{2\pi\sqrt{Re_\omega}}C_l' \quad (17)$$

where C_l' is lift coefficient; Re_p is particle Reynolds number; and $Re\omega$ is the vorticity Reynolds number.

According to Equation (17), C_l' =6.46 and 0≤Re_p≤Re_ω≤1.

$$C_l' = \begin{cases} 6.46\,f(Re_p, Re_\omega) & Re_p \le 40 \quad (18) \\ 6.46\times 0.0524(\beta Re)^{\frac{1}{2}} & 40 < Re_p \le 100 \quad (19) \end{cases}$$

where,

$$\beta = 0.5\left(\frac{Re_\omega}{Re_p}\right)$$

Fig. 2.

$$f(Re_p, Re_\omega) = (1-0.3314\beta^{0.5})e^{-0.1Re_p} + 0.3314\beta^{0.5} \quad (20)$$

The friction between the particles is the only source of stress in a denser solid phase packing at low shear speeds.

2. Materials and Methods

A. Materials

The system consists of several key components essential for efficient mud circulation and cuttings transport, including:

i. Mud Tank – Stores and conditions drilling fluid.
ii. Pump – Ensures fluid circulation through the system.
iii. Flow Meter – Measures the fluid flow rate for precise control.
iv. Inner Pipe – Facilitates fluid movement within the system.
v. ERT System – Provides electrical resistance tomography for monitoring fluid behaviour.
vi. Eccentricity Regulator – Adjusts the alignment of the drill pipe that is located within the annulus section.
vii. Annulus Section – Represents the spacing that exists between the drill pipe and wellbore, critical for fluid dynamics.
viii. Visualization Area – Enables direct observation of fluid and cuttings behavior.
ix. Motor for Inner Pipe Rotation – Controls rotational movement, influencing cuttings transport.
x. Return Line – Facilitates fluid recirculation back to the mud tank.
xi. Visualization Instruments – Aid in monitoring and analyzing the transport process.

B. Methods

1) Experimental Procedure

The experiment that is conducted features a 6.16m long annulus system, incorporating a transparent pipe with an acrylic outer pipe and an aluminium inner pipe, as depicted in Figure 2.1. The outer pipe has a diameter of 4.5 inches, while the inner pipe measures 2.5 inches in diameter. Using a manual regulator, the aluminium pipe can be adjusted to either a concentric or eccentric position relative to the outer pipe. Additionally, the inner pipe can rotate at speeds of up to 150 revolution per minute (RPM), accommodating any eccentric orientation.

The setup operates with a pressure not exceeding of 30 psi within the annulus under the liquid flow conditions.

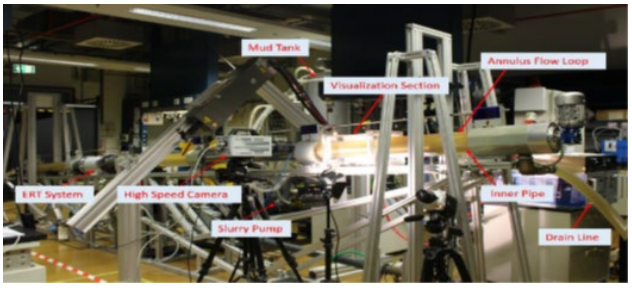

Fig. 3. A set-up of an experimental Flow loop

Figure 4 presents a simplified test section in a schematic set up. The experimental arrangement will operate within a closed-loop system, where the liquid and the solid cuttings are combined together using a high-speed agitator in the mud tank. Immediately a homogeneous slurry is formed, a slurry pump will be used to transports the two-phase mixture to the annulus section of well. The system's mass flow rate will be measured using a Coriolis meter.

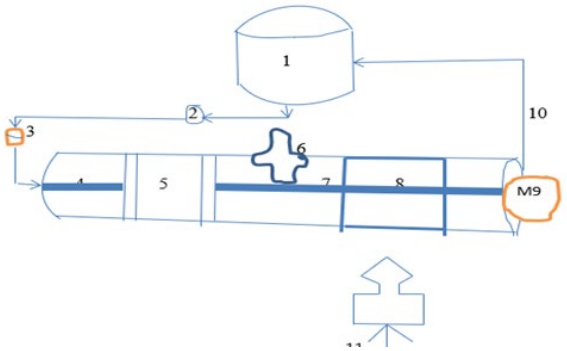

Fig. 4. A schematic experimental set-up for flow loop

Within the test set up, the fluid and the solid particles will pass through the ERT section, located approximately 2.5 meters from the inlet. The ERT system then estimates the instant solid volume fraction, while the section for visualization facilitates the assessment of bed height and the movement patterns of the solid bed. After the slurry has finished traversing the ERT section, pressure sensors, and the visualization area, a drain line is used to re-rout the slurry back to the mud tank at the test section outlet.

The main mud tank is filled with 300 liters of water at room temperature before the commencement of the experiment. Solid glass beads, ranging from 2.5 mm to 3.0 mm sizes, are utilized as drill cuttings. These beads have a density of approximately 2600 kg/m³. For the initial set of experiments, a solid concentration of 4% by weight was used, which conforms to a penetration rate of 85 ft/hr. The rate of penetration is estimated based on the method outlined by Larsen et al. (2017).

$$R_p\left(\frac{ft}{hr}\right) = Q_{inj}\left(\frac{ft^3}{sec}\right)\left(\frac{3600sec}{hr}\right)\left(\frac{1}{A_{hole}}\right)\left(\frac{1}{ft^2}\right) \quad (21)$$

The rate of penetration (RpR_p) is determined based on the volumetric injection of solid (QinjQ_{inj}) and the hole area (A hole A_{hole}) during drilling operations.

In this experiment, 300 liters of water were used in the mud tank, with 12 kg of solid material introduced into the system. Tests were conducted at varying slurry pump speeds, ranging from 500 revolution per minute (RPM) to 1000 revolution per minute (RPM), which corresponds to annular fluid velocities between 0.397 m/s and 0.818 m/s. At a lower pump rate, which ranges between 500 RPM - 600 RPM, a sand bed is formed at the entrance of the test section that is non-moving, which in turn prevents the solid dunes from reaching the visualization area. Consequently, the full experimental matrix commenced at a slurry pump rate of 700 RPM.

For every individual flow rate, the impact of the rotation of the inner pipe was evaluated. The experimental matrix data are summarized in Table 1. A total of 48 tests were conducted using a 4% solid concentration with three (3) eccentricities sizes (e = 0, 0.3, 0.6). Additionally, 24 experiments were conducted with an 8% solid concentration, varying the pump rate of the mud and testing two (2) annular orientations (e = 0, 0.3). Across the entire test cases, the ERT system estimated factions of annular volume, while the visualization system recorded video footage capturing the solid bed height, the duration of the movement of the bed, and movement patterns of the particles.

Table 1
The details of experimental test matrix

Matrix No	Pump Rate, (RPM)	Hole Eccentricity	Solid Volume Fraction	Drill Pipe Rotation (RPM)	Number of Test Conducted
	700	0, 0.3, 0.6	4%	0, 40, 80, 120	12
	800	0, 0.3, 0.6	4%	0, 40, 80, 120	12
	900	0, 0.3, 0.6	4%	0, 40, 80, 120	12
	1000	0, 0.3, 0.6	4%	0, 40, 80, 120	12
	800	0, 0.3	8%	0, 40, 80, 120	8
	900	0, 0.3	8%	0, 40, 80, 120	8
	1000	0, 0.3	8%	0, 40, 80, 120	8

2) Design of Experiment (DOE)

To analyze the influence of key factors and their interactions, a detailed list of items affecting transportation of fluid was compiled based on prior research. Before initiating simulation runs, the experimental design (DOE) method is applied to ensure systematic evaluation. A well-structured experimental design enables the identification of significant interactions between multiple input variables, enhancing the accuracy and reliability of the study.

Previous hole-cleaning studies demonstrate that numerous parameters influencing the cuttings transport efficiency. Table 2 presents key items and their respective ranges, as observed in previous research (Han et al., 2010; Ozbayoglu et al., 2008; Sifferman et al., 2013). The primary goal is to optimize cuttings transport capability.

Table 2
Key parameters selected for DOE

Subgroup	Category	Parameter	Tested Range	
			Minimum	Maximum
1	Fluid Rheology	Consistency Index (k), Pa.S^n	0.3	0.7
		Flow Behavior Index (n)	0.3	0.7
		Yield Stress (ro), Pa	0	4
2	Operational Parameters	Inner Pipe Rotation, rpm	10	80
		Mud Velocity, m/s	0.494	0.988
3	Cuttings Size and Annular Space	Cuttings Size, mm	1	5
		Diameter Ratio, (D_p/D_h)	0.44	0.89
		Eccentricity	0	0.7

To achieve the primary goal of optimizing cutting transport capability, a 2-level factorial experimental set-up is implemented. Items are systematically grouped into 3 sub-categories based on their domain knowledge, as detailed in Table.2.

At the outset, experiments are conducted by systematically varying the individual items within each of the group to determine which of the factors has the greatest influence on transportation of cuttings. Once the most significant items from all separate subgroups are identified, a subsequent set of experiments is carried out using these selected parameters to establish the process condition and optimal operating conditions. Additionally, a sensitivity analysis is performed to evaluate the individual effects of each item on the efficiency of cuttings transportation in an oil and gas drilling operation.

3) Setup of Simulation

This research considers a 6.4 meter (≈ 21 ft) horizontal annular test section, consisting of an outer pipe with a diameter of 2.91 inches and an inner pipe nominal diameter measuring 1.85 inches. The hydrodynamic entrance length (LhL_h) is utilized in determining the length of the test section, which represents the minimum distance required to establish a fully developed flow across all tested flow rate of the fluid and rheological conditions.

Since no well-established entrance length for solid-liquid flow in an annulus section exists in the literature, the estimation is performed using a single-phase flow model, as described in previous studies (Masuda, 2000).

$$L_{h,lam} = 0.05R_eD \quad (23)$$

$$L_{h,turb} = 4.4DR_e^{\frac{1}{6}} \quad (24)$$

In horizontal drilling, the weight of the drill pipe can help the development of an eccentric annulus, thereby causing it to settle against the borehole wall. The eccentricity is defined by the drill pipe relative position within the annulus. This study examines three distinct annular orientations: a concentric configuration (e = 0) and two eccentric conditions (e = 0.4 and e = 0.7).

The size and the quality of the mesh play a crucial role in Computational Fluid Dynamics studies, directly impacting accuracy and computational efficiency. For this simulation, a structured hexahedral mesh is utilized for the sake of the simplicity of the annular geometry.

To identify the right mesh size that would balance accuracy and computational resource efficiency, grid independence research is conducted across all geometric conditions. The grid study within the horizontal annulus section is validated using water with a velocity of 1.0 m/s, and the corresponding pressure drop is estimated.

Among various meshing techniques, face meshing and edge sizing are applied at the inlet boundaries and the outlet boundaries to ensure precise representation of boundary conditions. Multiple combinations of face division and edge sizing are tested to determine the ideal properties of the mesh.

The analysis of the grid independence reveals that for this annular diameter, increasing face division beyond 20 does not lead to further improvements in mesh quality. However, adjusting edge sizing results in a gradual enhancement the quality of the mesh, particularly in terms of skewness and orthogonal quality.

4) The Simulation Algorithm

The simulation process begins with;

i. The appropriate geometry selection
ii. Meshing
iii. Grid independence research

This study ensures that whichever mesh is chosen, that it provides reliable results without complexity arising from unnecessary computation.

The Eulerian model, recognized as one of the most advanced multiphase flow models in ANSYS Fluent, is employed in this research. This model solves a set of ‘n’ momentum and continuity equations for each phase, enabling a detailed analysis of interphase interactions. The coupling between phases is achieved through pressure and interphase exchange coefficients.

For a solid to liquid granular flow, the required properties are derived from the application of kinetic theory (Fluent, 2015). To ensure accuracy, the convergence of the solution is verified for each simulation run.

The finite volume method is utilized in this simulation study to discretize the flow equations, implemented through the commercial simulator Ansys Fluent v. 17.2. For pressure-velocity coupling, the Phase Coupled SIMPLE scheme is applied, while the QUICK scheme is utilized in the discretization of momentum equations. These methods are selected for their ability to efficiently solve conservation equations (mass and momentum) with reliable stability and convergence across the control volume and computational grid.

The convergence criteria for residuals are set at 10−410^{-4} for continuity and 10-310^{-3} for other variables to ensure accurate numerical results. Additionally, since solution convergence speed is influenced by under-relaxation factors,

adjustments are made to the continuity and solid volume fraction parameters to accelerate solution attainment.

3. Conclusion

This study presents a comprehensive investigation of cuttings transport behaviour in horizontal drilling operations through a combination of experimental analysis, simulation, and design of experiments (DOE). The results demonstrate that annular geometry, fluid velocity, and pipe eccentricity significantly influence pressure drop and cuttings transport efficiency. Increased fluid velocity enhances both cuttings velocity and overall transport, while higher eccentricity alters flow distribution and pressure characteristics. The integration of CFD simulation with experimental validation ensures reliability and deeper insight into multiphase flow dynamics. Sensitivity analysis further identifies key parameters governing efficient hole cleaning. Overall, the study provides valuable guidelines for optimizing drilling fluid design and operational conditions, contributing to improved hole cleaning performance, reduced operational risks, and enhanced efficiency in horizontal drilling systems.

References

[1] Fluent, (2015). ANSYS FLUENT User's Guide 15317, 2794.
[2] Han, S., Woo, N., Kim, Y. (2010) A study on cuttings transport in drilling fluids with inclined annulus. WIT Transactions on Engineering Sciences, 120, 95 - 101
[3] Hu, W., Zhang, J., Guan, N., Zhang, Y., Xu, B., Zhu, H. (2024). Optimization of wellbore annulus cleaning tool based on CFD-DEM and Box-Behnken design. E3S Web of Conferences 573, 1 – 6
[4] Huque, M.M. (2022). Systematic investigation of cuttings transport behaviour in horizontal and inclined drilling operation. Memorial University of Newfoundland, 1 – 310
[5] Inc. ANSYS, (2013). ANSYS FLUENT Theory Guide. Release 18.2 15317, 373–464. https://doi.org/10.1016/0140-3664(87)90311-2
[6] Mei, R., Klausner, J.F. (2014). Shear Lift Force on Spherical Bubbles. Int. j. Heat Fluid Flow 15, 62–65. https://doi.org/10.1016/0142-727X(94)90031-0
[7] Ozbayoglu, M.E., Miska, Z.S., Reed, T., Takach, N. (2008). Cuttings transport with foam in horizontal & highly-inclined wellbores. SPE 79856, SPE/IADC Drilling Conference, Amsterdam, Netherlands
[8] Ozbayoglu, E.M., Ettehadi-Osgouei, R., Ozbayoglu, M.A., Yuksel, E.H. (2012). Hole cleaning performance of gasified drilling fluids in horizontal well sections. SPE j. 17, 912–923. https://doi.org/10.2118/131378-PA
[9] Saffman, P.G., (2013). The lift on a small sphere in a slow shear flow. j. Fluid Mech. 22, 385. https://doi.org/10.1017/S0022112065000824
[10] Sifferman, T.R., Myers, G.M., Haden, E.L. (2019). Drill cutting transport in full scale vertical annuli. j. Pet Tech 26 (11): 1295-1302. SPE-4514-PA. http://dx.doi.org/10.2118/4514-PA.
[11] Sifferman, T.R., Myers, G.M., Haden, E.L., Wahl, H.A. (2013). Drill cuttings transport in full scale vertical annuli, in: 48th Annular Fall Meeting of the Society of Petroleum Engineers of AIME. Las Vegas, 30 Sept- 3 Oct. https://doi.org/10.2118/4514-MS
[12] Wei, X., Miska, S.Z., Takach, N.E., Bern, P., Kenny, P. (2018). The effect of drill pipe rotation on annular frictional pressure. j. Energy Resour. Technol. ASME https://doi.org/10.1115/1.2795011
[13] Larsen, T.I., Pilehvari, A.A., and Azar, J.J. (2017). Development of a new cuttings transport model for high-angle wellbores including horizontal wells. Presented at the SPE Rocky Mountain Regional/Low Permeability Reservoir Symposium, Denver, 12–14 April. SPE-25872-MS
[14] Masuda, Y., Doan, Q., Oguztoreli, M., Naganawa, S., Yonezawa, T., Kbayashi, A., Kamp, A. (2000). Critical cuttings transport velocity in inclined annulus: Experimental Studies and Numerical Simulation, in: SPE/CIM International Conference on Horizontal Well Technology. Calgary, Alberta, Canada, 6-8 November. https://doi.org/10.2118/65502-MS